

Article

Effect of Diethanol-Isopropanolamine and Typical Supplementary Cementitious Materials on the Hydration Mechanism of BOF Slag Cement Pastes

Hongyu Wang^{1,2}, Xiaowei Gu^{1,2,*}, Xiaochuan Xu^{1,2}, Jianping Liu^{3,*}, Zhenguo Zhu^{1,2} and Shenyu Wang^{1,2}

- ¹ Science and Technology Innovation Center of Smart Water and Resource Environment, Northeastern University, Shenyang 110819, China; 2010415@stu.neu.edu.cn (H.W.); xuxiaochuan@mail.neu.edu.cn (X.X.); 2190073@stu.neu.edu.cn (Z.Z.); 2100996@stu.neu.edu.cn (S.W.)
² Liaoning Institute of Technological Innovation in Solid Waste Utilization, Shenyang 110819, China
³ School of Architecture and Civil Engineering, Shenyang University of Technology, Shenyang 110870, China
* Correspondence: guxiaowei@mail.neu.edu.cn (X.G.); liujianping024@163.com (J.L.)

Abstract: This study investigated the effects of lithium slag and iron tailings on the hydration mechanism of Basic Oxygen Furnace (BOF) slag cement paste with the addition of 0.06% diethanol-isopropanolamine (DEIPA). This study examined the fluidity, compressive strength, pore solution pH, and hydration products of BOF slag-based composite cementitious materials. The results showed that DEIPA facilitated the conversion from ettringite (AFt) to monosulphate (AFm) and improved the early compressive strength of the BOF slag–cement mortar. Incorporating lithium slag into the DEIPA-containing BOF slag–cement system promoted AFt formation, increased calcium-silicate-hydrate production, and enhanced the microstructure. BOF slag, lithium slag, and iron tailings exhibit synergistic effects in cement pastes. BOF slag and lithium slag provided the reactive components SiO₂ and Al₂O₃. In the early hydration stages, the iron tailings primarily served as fillers, accelerating the system's reactions.

Keywords: supplementary cementitious materials; diethanol-isopropanolamine; pozzolanic reaction; BOF slag; compressive strength



Citation: Wang, H.; Gu, X.; Xu, X.; Liu, J.; Zhu, Z.; Wang, S. Effect of Diethanol-Isopropanolamine and Typical Supplementary Cementitious Materials on the Hydration Mechanism of BOF Slag Cement Pastes. *Buildings* **2024**, *14*, 1268. <https://doi.org/10.3390/buildings14051268>

Academic Editor: Denny Coffetti

Received: 27 February 2024

Revised: 25 March 2024

Accepted: 25 March 2024

Published: 1 May 2024



Copyright: © 2024 by the authors. Licensee MDPI, Basel, Switzerland. This article is an open access article distributed under the terms and conditions of the Creative Commons Attribution (CC BY) license (<https://creativecommons.org/licenses/by/4.0/>).

1. Introduction

In China, the rapid development of the iron and steel industry caused a significant increase in the production of steel slag. However, the comprehensive utilization rate is only about 30%, signifying a substantial disparity with developed countries [1,2]. More than 70% of the steel slag produced in China belongs to Basic Oxygen Furnace (BOF) slag. BOF slag contains C₂S and C₃S and has a large storage capacity, which ensures that it can be used as a basic condition for concrete admixtures [3,4]. Nevertheless, multiple factors impede the large-scale substitution of BOF slag for cement [5–9]. The main reasons are as follows: the silicate mineral content in BOF slag is relatively low, and it contains impurities such as FeO and MgO, resulting in lower early strength [7,10]. Previous studies have indicated that the dosing with BOF slag generally does not exceed 20 wt% under standard curing conditions [5]. This is because BOF slag can reduce the pH of the pore solution and impede the reaction between C₃S and Ca(OH)₂ [11]. Therefore, improving the early activity of BOF slag is the essential to increase its utilization.

BOF slag contains significant quantities of f-CaO and f-MgO, which participate in hydration reactions, leading to reduced stability [10,12]. Researchers have employed diverse activation methods to enhance the reactivity of BOF slag [13–18]. Sun et al. [19] studied the effects of dry and wet grinding on the activity of steel slag, finding that wet grinding surpasses dry grinding in effectiveness and energy efficiency. Zhang et al. [20] researched performance optimization in a steel slag–cement mortar with different alkaline activators and

found that alkaline activators can promote the decomposition of the vitreous structure in steel slag and improve its reactivity. The production of strong alkalis such as sodium hydroxide will produce a large amount of carbon dioxide emissions, increasing the cost of BOF slag utilization [21]. Huo et al. [22,23] employed phosphoric acid and formic acid to pretreat steel slag, enhancing its surface roughness and initial reactivity. Zepper et al. [3] analyzed the hydration effects of BOF slag under autoclave conditions and its application in dense autoclaved bricks. Wang et al. [24] proposed that organic alcohol amines enhance the dissolution of steel slag and the hydration of C_3S and C_2S , noting that diethanol-isopropanolamine (DEIPA) remains the longest in the liquid phase. The addition of organic alcohol amines, such as triisopropanolamine (TIPA) [25,26] and triethanolamine (TEA) [27], can accelerate dissolution and promote the hydration process. There are many studies on TEA and TIPA in the existing literature, but there are few studies on DEIPA [28,29].

Based on the synergistic effect of multi-source solid waste and BOF slag in chemical composition and mineral phase composition, the preparation of BOF slag-based composite SCMs is of great value for promoting the large-scale utilization of steel slag. Zhang et al. [8] added nano- SiO_2 into a cement mortar containing steel slag to improve its compressive strength. Liu et al. [30] prepared composite SCMs by grinding steel slag and silica fume, which promoted the consumption of $Ca(OH)_2$ and improved the microstructure of the system. Zhang et al. [31] studied the replacement of cement with steel slag and waste glass powder, and accelerated the hydration reaction using an autoclave. Hao et al. [32] prepared cementitious materials using steel slag, red mud, and desulfurization gypsum, and found that the alkali in red mud accelerated the reaction rate of the silicates in steel slag. SCMs mainly appear in the form of $CaO-Al_2O_3-SiO_2$ matrix material, and the ratio of Ca, Al, and Si has a significant effect on the performance of calcium-silicate-hydrate (C-S-H) [33,34]. The filler and pozzolanic properties of SCMs in cement-based materials add to the research complexity [35]. BOF slag belongs to calcium-phase material, while nano- SiO_2 , silica fume, and waste glass powder belong to silicon-phase material, and red mud, metakaolin, and lithium slag belong to aluminum-phase material [36–38]. Therefore, the co-blending of typical aluminum and silicon solid waste with steel slag is of great value for the scale-up of solid waste utilization.

Iron tailings, an industrial by-product of mineral processing, constitute a major category of bulky industrial solid waste [39–41]. Advancements in mineral processing technology have reduced the particle size of iron tailings [42]. Fine-grained iron tailings can contribute to air pollution and pose health risks [43]. In addition, iron tailings take up a large amount of land and tailings dams are expensive to maintain [44,45]. Milled iron tailings exhibit cementitious properties and serve as effective fillers, making them suitable for use as SCMs [46]. Lithium slag is a waste residue produced during the production of lithium carbonate [47]. With the wide application of lithium batteries, the production of lithium slag is also increasing [48]. Most of Al_2O_3 and SiO_2 in lithium slag mainly exist in an amorphous form and can be used as SCMs [48]. However, the high sulfate content in lithium slag can significantly affect the performance of cement-based materials [49,50].

The synergistic effect of multiple SCMs together replacing cement can take advantage of the benefits of solid waste materials. DEIPA can promote the hydration of BOF slag particles in cementitious materials. However, the promotion of BOF slag cement systems by DEIPA and typical SCMs has not been studied. This study selected high-silicon iron tailings (silicon phase) and lithium slag (aluminum phase) to prepare three BOF slag-based composite cementitious materials, analyzing the effects of DEIPA and typical SCMs on their hydration properties. The fluidity and compressive strength of composite mortar were studied. The samples were analyzed for hydration products by their pH value, XRD, FTIR, TG-DTG, and SEM. The hydration mechanism of the BOF slag-based composite system was discussed.

2. Materials and Methods

2.1. Materials

In this study, ordinary Portland cement (P·O 42.5), BOF slag, lithium slag, and iron tailings were utilized as binders. BOF slag was provided by Shanghai Baowu Group

(Shanghai, China). Lithium slag was sourced from Jiangxi lithium salt plant (Jiangxi, China) in China. Iron tailings were acquired from Benxi Iron Mine (Benxi, China) in Liaoning Province, China. Table 1 shows the chemical composition of the raw materials. The iron tailings contain 62.26% SiO_2 , indicating high silicon variety. The Al_2O_3 content in lithium slag is 22.32%. The cementitious activity of lithium slag increases with the content of Al_2O_3 , its primary active component. The mineral composition of the raw materials is shown in Figure 1. The diffraction peaks of the iron tailings are mainly sharp quartz peaks, indicating a high degree of crystallization in the iron tailings. Figure 2 shows the particle size distribution of cement, BOF slag, lithium slag, and iron tailings. The median particle size of SCMs is smaller than that of cement. Fine-grained iron tailings were obtained through mechanical grinding. The molecular structure of DEIPA is shown in Figure 3. The purity of DEIPA used is 85%. Deionized water is used as the experimental water. The sand used is standard sand.

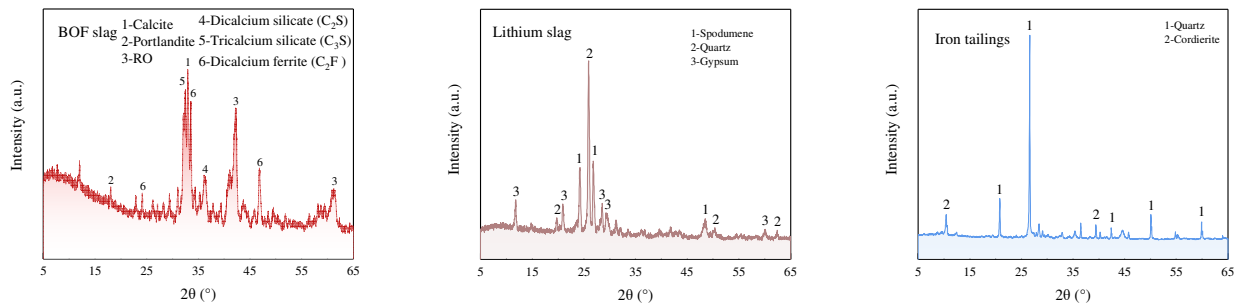


Figure 1. XRD pattern of raw materials.

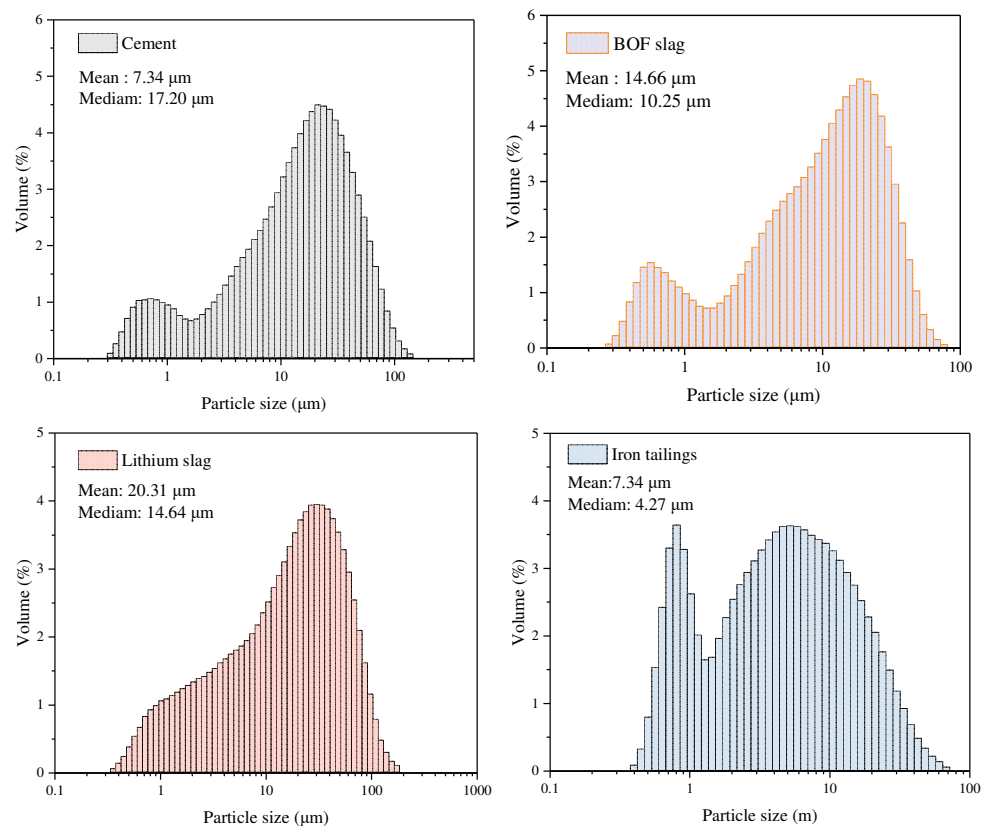


Figure 2. Particle size distribution of raw materials.

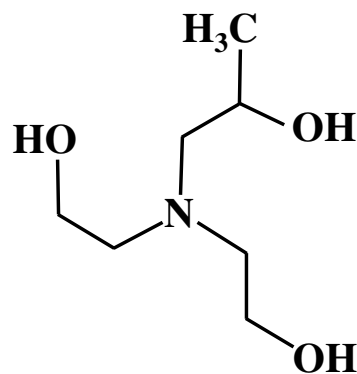


Figure 3. The structural formula of DEIPA.

Table 1. Chemical composition of raw materials (wt%).

	CaO	Al ₂ O ₃	SiO ₂	Fe ₂ O ₃	K ₂ O	Na ₂ O	MgO	P ₂ O ₅	SO ₃
Cement	54.01	9.01	25.53	3.36	0.94	0.03	3.28	0.15	2.859
BOF slag	42.65	2.53	15.20	27.54	0.06	0.02	6.05	1.97	0.12
Lithium slag	9.51	22.32	58.36	1.42	0.67	0.02	0.39	0.11	6.91
Iron tailings	7.76	4.78	62.26	14.37	1.40	1.34	6.33	0.44	0.48

2.2. Procedure

2.2.1. Preparation of Cement Mortar

Cement mortar preparation followed the Chinese standard GB/T 17671-2021 [41]. As shown in Table 2, SCMs account for 30% of the binder material. The C-S and C-S-D samples were analyzed to evaluate the effect of DEIPA on the BOF slag–cement system. C-SL-D, C-SI-D, and C-SLI-D are multi-component cementitious materials comprising BOF slag, lithium slag, and iron tailings, with DEIPA as an additive. In the C-SL-D system, the mass ratio of BOF slag to lithium slag is 1:2 [51]. In the C-SI-D system, the mass ratio of BOF slag to iron tailings is 2:1 [52]. In the C-SLI-D system, the mass ratio of BOF slag, lithium slag, and iron tailings is 5:10:3. The cement and SCMs were slowly stirred in a mixer for 3 min to homogenize the material. Then, 0.06% DEIPA of the cementitious material was pre-dissolved in water. The DEIPA dosage was selected with reference to the literature [53]. The mixed cement mortar was molded in a 40 × 40 × 160 mm mold. The test blocks were placed in a standard curing room (98% RH, 20 °C). The samples were demolded and water cured after 24 h of curing.

Table 2. Mixture proportions of samples.

NO.	Binder/g				DEIPA/g	Water/g	Sand/g
	OPC	SS	LS	IOT			
C-S	315	135	/	/	/	225	1350
C-S-D	315	135	/	/	0.27	225	1350
C-SL-D	315	45	90	/	0.27	225	1350
C-SI-D	315	90	/	45	0.27	225	1350
C-SLI-D	315	35	70	21	0.27	225	1350

Note: “C” represents Cement, “D” represents DEIPA, “S” represents BOF slag, “L” represents lithium slag, and “I” represents iron tailings.

2.2.2. Preparation of Cement Paste

The cement and SCMs were prepared according to the ratio of Table 2 to prepare a cement paste. The water–binder ratio of the samples was 0.5. After mixing DEIPA in water, the cementitious material was stirred and cast into a 20 × 20 × 20 mm mold. The cement paste was demolded after 24 h of standard and water curing. After reaching the set curing

age, the cement paste was broken into small pieces, and then the hydration was terminated with anhydrous ethanol. The sample was manually ground to a powder. After sieving through a 45 μm mesh, the prepared powder samples underwent analysis for pore solution pH, XRD, FTIR, and TG-DTG.

2.3. Testing Methods

2.3.1. Flowability

The fluidity of fresh mortar was measured in accordance with GB/T 2419-2016 [54]. A truncated cone mold with a height of 60 mm and diameters of 70 mm at the top and 100 mm at the base was used. The fresh mortar was filled into the mold in two layers, after which the mold was swiftly removed to let the mortar spread freely. The diameter of mortar after dispersion was measured after 25 rounds of vibration. The diameters were measured in two perpendicular directions and their average was recorded as the result.

2.3.2. Compressive Strength

The compressive strength test process of cement mortar was carried out according to the Chinese standard GB/T 17671-2021 [55]. The compressive strength of $40 \times 40 \times 160$ mm mortar specimens cured to 3 d, 7 d, and 28 d was tested by YAW-300 pressure testing machine at a loading speed of 2.4 kN/s. Compressive strength was averaged by removing outliers from the six results.

2.3.3. Pore Solution pH

The pore solution pH of the hardened cement paste is closely related to the degree of hydration reaction of the system and the stability of the hydration products [56]. This study employed the solid–liquid extraction method to determine the pore solution pH of the cement paste at different curing ages. The solid–liquid extraction method is favored for its simplicity and cost-effectiveness. The method of determining the pH value of the pore fluid was as follows: (a) The 3 d, 7 d, and 28 d hardened slurries were terminally hydrated with anhydrous ethanol and dried at 40 °C. (b) The sample powder was diluted with deionized water at a ratio of 1:10 and stirred with a magnetic stirrer at 1000 rpm for 5 min. (c) The solid–liquid mixture was filtered through filter paper. (d) Using a pH meter (pH-100B), the pH value of the upper layer was measured.

2.3.4. Hydration Products

The hardened paste cured for 7 days was used for hydration product analysis. The hardened paste was broken into small pieces, the hydration was terminated, and the powder was ground into a powder for the characterization of the hydration product type and microstructure. The mineral composition of early cement paste hydration products was tested using Rigaku Ultima IV diffractometer at a test voltage of 40 kV and a current of 40 mA. The 2θ range is 5° to 75° and the scanning speed is 10°/min.

The chemical bonds of the hydration products of the hardened paste were characterized by infrared spectroscopy (Thermo Scientific Nicolet iS20, Waltham, MA, USA). The sample was thoroughly ground with KBr powder and pressed into thin sheets. The wavenumber range of data acquisition is 400–4000 cm^{-1} , the resolution is 4 cm^{-1} , and the number of scans is 32 times.

The hydration products were qualitatively and quantitatively detected by thermogravimetric analyzer (TG 209 F3Tarsus, Bayern, Germany). The sample underwent heating from 40 °C to 950 °C at a rate of 20 °C/min. After the balance was cleared, the samples were loaded into a corundum crucible and experiments were performed in a nitrogen atmosphere.

The microstructural morphology and elemental distribution of the hardened cement paste were characterized using scanning electron microscopy (ZEISS Gemini 300, Oberkochen, Germany). The sheet sample was glued to the conductive adhesive and

sprayed with gold for 45 s, and the gold spray was 10 mA. An acceleration voltage of 3 kV was applied during topographic imaging.

3. Results and Discussion

3.1. Flowability

Figure 4 shows the flow results of fresh cement mortar with different ratios. The flowability of the C-S and C-S-D samples were 193 mm and 213 mm, suggesting that DEIPA incorporation into the BOF slag–cement system markedly enhances the fluidity of the cement mortar. DEIPA effectively dispersed BOF slag and cement and improved cement paste fluidity by reducing the interaction force between particles. The fluidity of the C-SL-D and C-SI-D samples was 200 mm and 209 mm, respectively, both lower than that of the C-S-D sample. Both lithium slag and iron tailings led to a decrease in mortar fluidity, but the effect mechanisms were not the same. Lithium slag is a porous structure with some water absorption [51]. Iron tailings with small particle sizes have a large specific area and demand a large amount of water to reach a plastic state [52]. The fluidity of the C-SLI-D sample was 6 mm higher than that of the C-S sample. The fluidity of the mixed mortar was better than that of the BOF slag–cement system after the combined replacement of cement by BOF slag, lithium slag, and iron tailings in the presence of DEIPA.

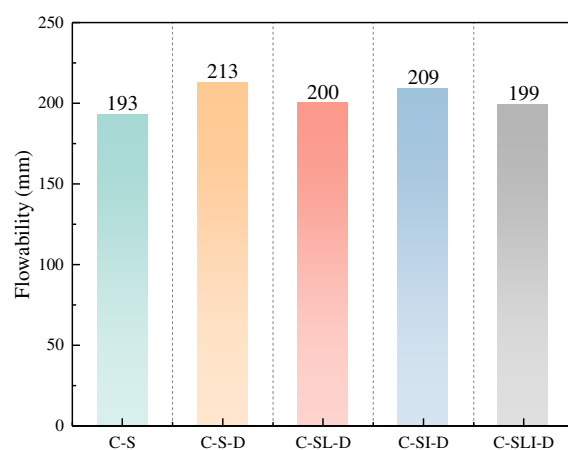


Figure 4. Flowability of samples with different mixing ratios.

3.2. Mechanical Properties

Figure 5 shows the compressive strength of mortars containing DEIPA and different SCMs. The compressive strength of the C-S-D sample, which was cured for 7 d, was 11.7% higher compared to the C-S sample. This indicates that DEIPA has a positive effect on the early response of BOF slag–cement, which is consistent with the findings in the literature [57]. The addition of lithium slag and iron tailings further enhanced the compressive strength of the cement mortar at various ages. The compressive strength of the C-SL-D, C-SI-D, and C-SLI-D samples increased by 11.1%, 1.2%, and 12.2%, respectively, when compared with that of the C-S-D sample at 3 d. The addition of iron tailings had a minimal impact on the early-stage enhancement of the BOF slag–cement system, whereas lithium slag had a significant effect. This was attributed to the high content of SO_4^{2-} in the lithium slag, which could promote the formation of ettringite (Aft) [58]. The mortar compressive strength of C-SLI-D was higher than that of C-SL-D, which was due to the microaggregate effect and nucleation of iron tailings, promoting the reaction between BOF slag and lithium slag.

In the presence of DEIPA, the compressive strength of samples containing binary and ternary SCMs with a curing age of up to 7 d was higher than that of the BOF slag–cement system. The compressive strength of the C-SI-D sample was lower compared to C-S-D, indicating higher early reactivity in BOF slag than in iron tailings. Among the samples cured for 7 days, C-SL-D had the highest compressive strength of 34.71 MPa. The interaction

of BOF slag with lithium slag promoted the early hydration of the mixed mortar. The 28-day compressive strength results have a similar pattern to the early compressive strength. The 28-day compressive strength of the C-SLI-D sample reached 51.17 MPa, which was the highest among all the samples.

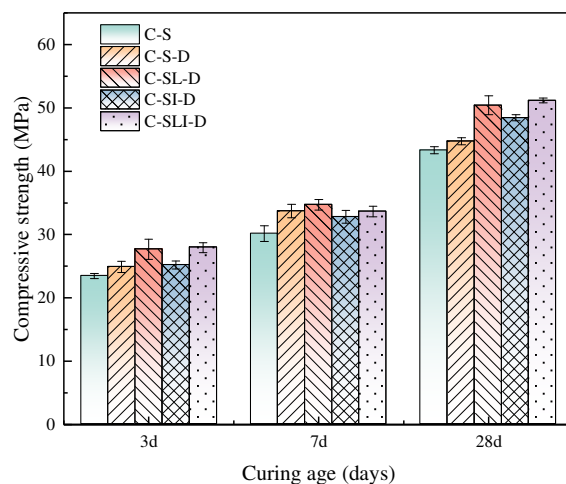


Figure 5. Compressive strength of mortar blends containing DEIPA and different SCMs.

3.3. pH Value

Figure 6 shows the pore solution pH of hardened cement pastes with different mixing ratios. In Figure 6, the pH level of the pore solution in the hardened cement paste exhibits a gradual reduction correlating with prolonged curing durations. This suggests that SCMs play the role of filling mainly in the early stage of the hydration reaction. The higher level of $\text{Ca}(\text{OH})_2$ consumed by the SCMs with a high level of cementitious activity led to a subsequent decrease in the pH of the pore solution of the hardened paste occurring at a later stage. The addition of DEIPA resulted in a decrease in the pore solution pH across various ages of the C-S samples. DEIPA promoted the hydration of BOF slag and cement, and BOF slag reacted with more $\text{Ca}(\text{OH})_2$ in a pozzolanic reaction, leading to a decrease in pH, which is consistent with the compressive strength results. The C-SL-D sample exhibited the lowest pH at both 7 and 28 days. This indicates that a strong pozzolanic reaction occurred in the BOF slag-lithium slag-cement composite system. The pH of the 3-day and 7-day hardened pastes of the C-SI-D sample was higher than that of C-S-D. Iron tailings cannot promote the early pozzolanic reaction of the BOF slag-cement system. Iron tailings and DEIPA promoted the hydration reaction of the BOF slag-cement system at the late stage of the hydration reaction. The pore solution pH of the 3-days hardened paste of the C-SLI-D sample was 12.14, which was the lowest among all the samples. In the presence of DEIPA, BOF slag, lithium slag, and iron tailings have a synergistic effect in the cementitious system, thus accelerating the early hydration reaction.

3.4. XRD Analysis

The XRD diffraction pattern of the hardened cement paste cured for 7 d is shown in Figure 7. In Figure 7a, the hydration products of the composite system were mainly ettringite (AFt), monosulfate (AFm), quartz, calcite, and C-S-H. AFm phases (hemihydrate and monohydrate) were also observed, which were associated with the presence of calcium carbonate [59]. The AFm phase served to stabilize AFt, which is consistent with the formulation in the literature [60]. RO phase, spodumene ($\text{LiAlSi}_2\text{O}_6$), and quartz were unreacted components of BOF slag, lithium slag, and iron tailings, respectively. The C-SL-D sample exhibited the highest C-S-H, suggesting that BOF slag and lithium slag were involved in the pozzolanic reaction, producing additional C-S-H, consistent with the results for compressive strength. The XRD diffraction pattern was locally enlarged to obtain the enlarged images of the characteristic peaks of AFt and $\text{Ca}(\text{OH})_2$, as shown in Figure 7b,c.

In Figure 7b, the Aft diffraction peaks of C-S-D were slightly lower than those of C-S. The Aft diffraction peaks of the remaining samples were, in descending order, C-SLI-D, C-SL-D, and C-SI-D. The C-SLI-D sample displayed the highest Aft content, attributable to the SO_4^{2-} in lithium slag, which favors Aft formation. And a small amount of iron tailings had an accelerated effect on the reaction of the BOF slag-lithium slag-cement system. In Figure 7c, the $\text{Ca}(\text{OH})_2$ content of the composite paste decreased after DEIPA was added to the C-S system. This also demonstrated that DEIPA accelerated the pozzolanic reaction of BOF slag. The C-SLI-D sample exhibited the lowest $\text{Ca}(\text{OH})_2$ diffraction peaks, suggesting a synergistic effect of BOF slag, lithium slag, and iron tailings in the presence of DEIPA, which consumed more $\text{Ca}(\text{OH})_2$.

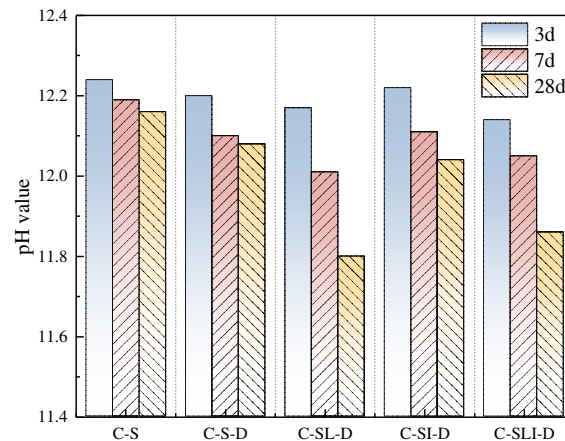


Figure 6. The pH value of pore fluid for samples with different mixing ratios.

3.5. FTIR Analysis

Figure 8 shows the FTIR spectra of hardened pastes containing different SCMs cured for 7 d in the presence of DEIPA. In Figure 8a, the distribution of the absorption peaks of chemical bonds in the hardened pastes was almost the same. The absorption bands near 3422 cm^{-1} and 1648 cm^{-1} were associated with the vibrations of O-H groups in water [56,61]. The peaks near 1419 cm^{-1} and 875 cm^{-1} were caused by the vibration of C-O groups in calcite [52]. This was related to the carbonization reaction of the sample curing process and the calcite contained in the raw material. The O-H bond in $\text{Ca}(\text{OH})_2$ exhibited an absorption peak at approximately 3643 cm^{-1} [62], as shown in Figure 8b. The highest transmittance of the C-SLI-D sample indicated the lower $\text{Ca}(\text{OH})_2$ content in the sample. This suggested that the presence of DEIPA in the cementitious system resulted in an increased consumption of $\text{Ca}(\text{OH})_2$ by BOF slag, lithium slag, and iron tailings, which was consistent with the findings from the XRD analysis. The Si-O-Si bond in C-S-H was around 979 cm^{-1} , as shown in Figure 8c. The transmittance of Si-O-Si groups was the highest and lowest value for the C-S and C-SL-D samples, respectively. This indicated that the addition of EDIPA and different SCMs increased the C-S-H content within the BOF slag-cement matrix.

3.6. TG-DTG Analysis

Figure 9 shows the TG and DTG curves of 7 d hardened cement pastes containing different SCMs. The mass loss of the sample responds to the total amount of hydration products in the hardened paste. In Figure 9a, the C-S-D sample exhibited a greater mass loss compared to the C-S sample. The hydration of the BOF slag-cement system increased in the presence of DEIPA and more hydration products were generated. The C-SL-D sample showed the maximum mass loss. This indicated a high degree of reaction between the BOF slag and lithium slag interaction in the presence of DEIPA, which was consistent with the XRD results. In Figure 9b, there are three distinct weight loss peaks in the DTG curves, representing the decomposition of hydration products (C-S-H, Aft, and AFm, $50\text{--}150\text{ }^\circ\text{C}$),

Ca(OH)_2 (400–500 °C), and calcite (650–750 °C), respectively. The peaks representing weight loss for the C-S-D samples exceeded those of the C-S samples around the 100 °C mark. This indicates that the BOF slag-cement system produced less of an AFt content and more of an AFm content after the addition of DEIPA. DEIPA accelerated the reaction of gypsum in the system, thus promoting the generation of AFm, which was consistent with the results of the literature [28]. The DEIPA content was constant and the Ca(OH)_2 mass loss peak in the composite system was reduced by the addition of lithium slag and iron tailings to the BOF slag-cement system. Among all the samples, the weight loss peak corresponding to Ca(OH)_2 in the C-SLI-D sample was the least pronounced. This indicates that BOF slag, lithium slag, and iron tailings consume more Ca(OH)_2 in the cementitious system, which is consistent with the XRD results.

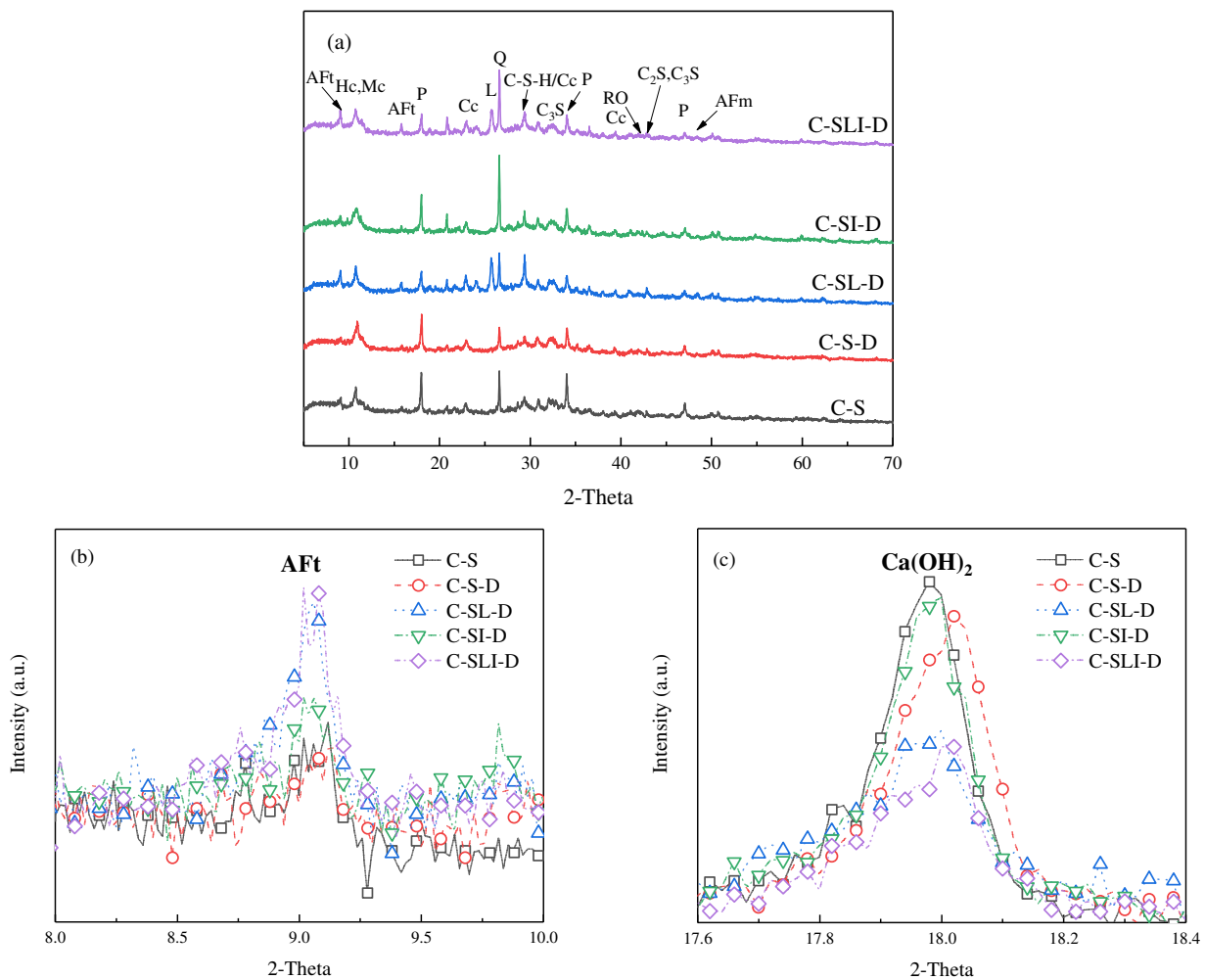


Figure 7. XRD patterns of the pastes at 7 d: (a) XRD patterns; (b) and (c) enlarged view. (Hc—Hemicarboaluminate (PDF#241-0221), Mc—Monocarboaluminate (PDF#41-02219), P— Ca(OH)_2 (PDF#04-0733), Cc—Calcite (PDF#47-1743), L— $\text{LiAlSi}_2\text{O}_6$ (PDF#39-0049), Q—Quartz (PDF#46-1045), AFt—Ettringite (PDF#41-1451)).

3.7. SEM Analysis

Figure 10 shows the SEM images and EDS face-scan results of 7-day hardened BOF slag-cement pastes with and without DEIPA. The C-S-D sample contains more types of hydration products than the C-S sample. In the C-S sample, the generated clustered C-S-H is dispersed and there is a large amount of flaky AFm in the cleavage. Acicular AFt, flaky Ca(OH)_2 , and fibrous and reticulated C-S-H surround the surface of unreacted BOF slag and cement particles in the C-S-D sample. EDS surface scanning revealed that the addition

of DEIPA resulted in a more homogeneous distribution of elemental calcium within the BOF slag-cement system. The elements silicon, aluminum, and oxygen show different abundances in the C-S-D samples, which is indicative of the presence of C-S-H gels and other hydration products [63–66].

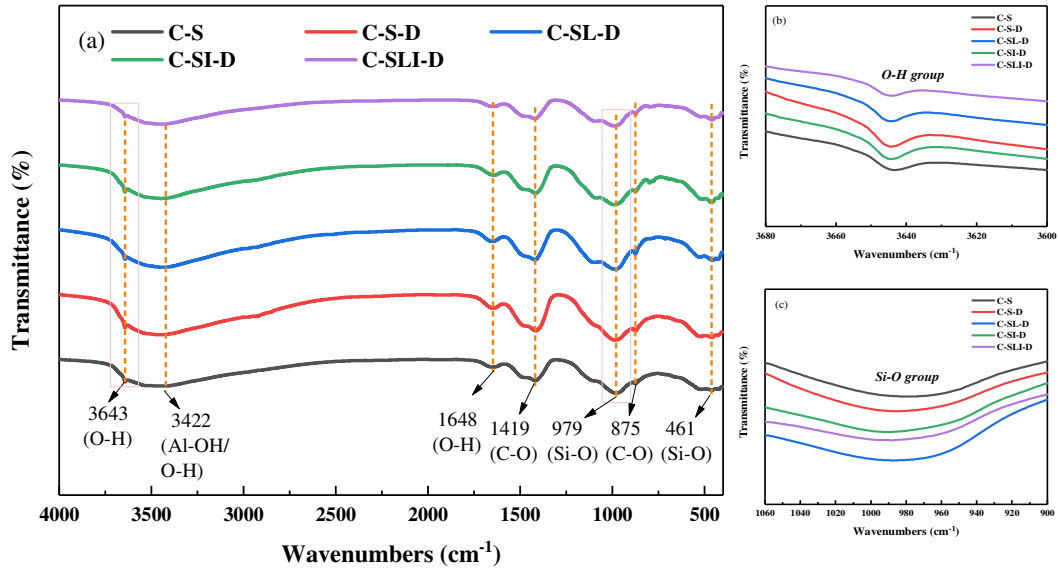


Figure 8. FTIR spectra of pastes at 7 d with different mixing ratios: (a) FTIR spectra (b) O-H group; (c) Si-O group.

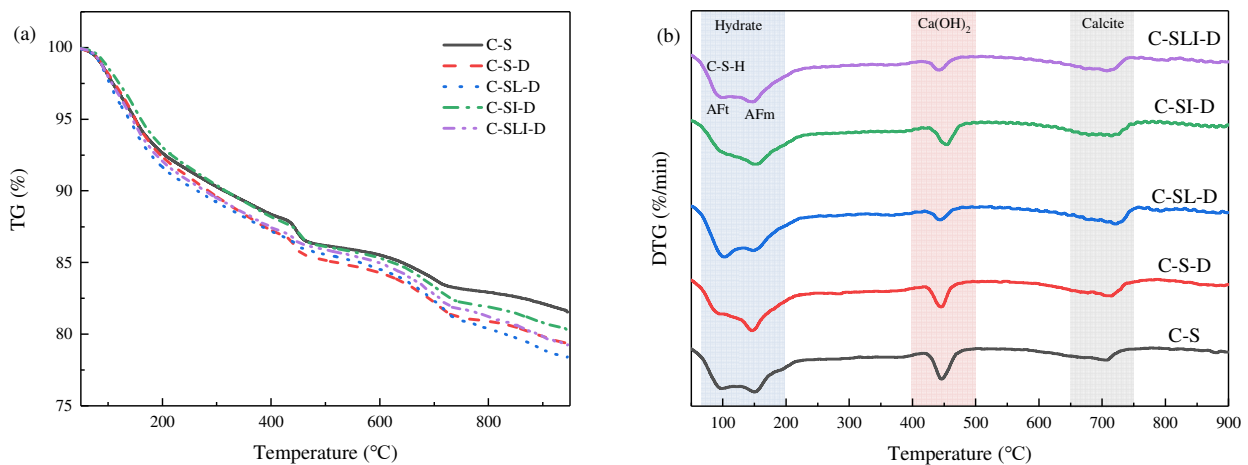


Figure 9. TG-DTG curves of hardened slurries containing different SCMs: (a) TG curves (b) DTG curves.

The microscopic morphology of 7 d hardened cement paste containing different SCMs in the presence of DEIPA is shown in Figure 11. The morphology of C-S-H generated in the composite system changed from fibrous to flocculent after the addition of lithium slag to C-S-D, as shown in Figure 11a,b. The complexity of the microscopic morphology of the BOF slag-cement system increased after the incorporation of lithium slag, which favored the filling of small pores. As shown in Figure 11c, the main hydration products of the BOF slag-iron tailings-cement system were needle-like AFt and fibrous C-S-H. Hexagonal sheet-like $\text{Ca}(\text{OH})_2$ was observed in the BOF slag-iron tailings cement system in samples containing DEIPA. This suggests that, at this specific mixing ratio, the SCMs consumed the least $\text{Ca}(\text{OH})_2$, aligning with the XRD findings. The ternary SCM cement paste (C-SLI-D) exhibited tighter packing between hydration products and unhydrated particles compared to binary SCM samples (C-SL-D and C-SI-D), as depicted in Figure 11d.

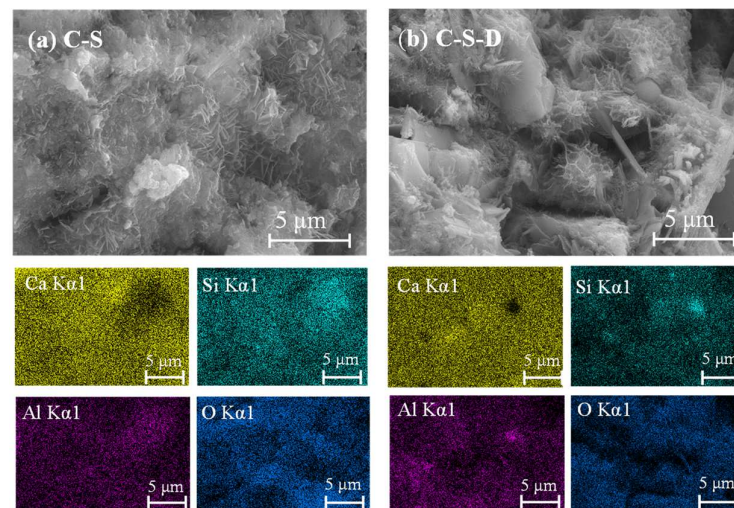


Figure 10. SEM images and elemental distribution of BOF slag-cement paste with and without DEIPA.

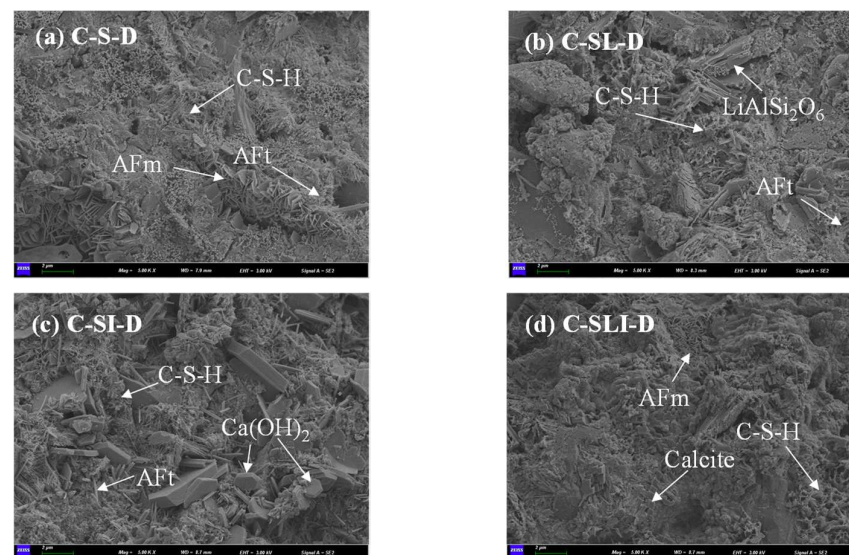
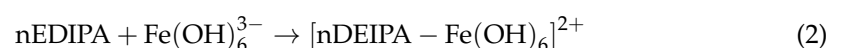
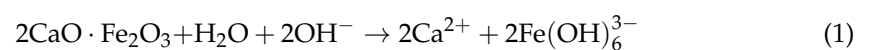
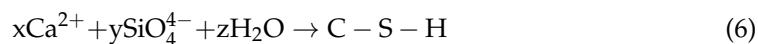
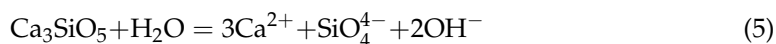


Figure 11. Microscopic morphology of cement pastes containing different SCMs.

3.8. Mechanical Analysis

This study analyzed the enhancement mechanism of a BOF slag-cement system by DEIPA and poly SCMs. Incorporating DEIPA into the BOF slag-cement system amplified the pozzolanic reactions, which in turn boosted the compressive strength of the cured mortar. The solubilization-promoting effect of DEIPA on the iron phase induced the formation of a large number of amine-iron complexes in the liquid phase of the composite paste. The chelation reaction of C_2F in BOF slag occurred as shown in Equations (1) and (2). The chelation reaction promoted the dissolution of C_4AF and advanced the initial hydration process of BOF slag and cement, as indicated by references [21,57]. The complexation reaction of Ca^{2+} is shown in Equations (3) and (4). The complexation of Ca^{2+} by DEIPA promoted the dispersion and dissolution of BOF slag and cement particles (Equations (5) and (6)). And, it promoted cement hydration and accelerated the transition from AFt to AFm (Figures 7 and 9).





A BOF slag cement mortar containing DEIPA was prepared using lithium slag and iron tailings with BOF slag. The BOF slag-cement system changed the morphology of C-S-H from fibrous to flocculent and improved the pore structure after incorporating lithium slag. The SO_3 contained in the lithium slag reacted with the aluminates to form AFt, thus improving the early strength [51]. The active component in the BOF slag was CaO, which provided Ca^{2+} for the generation of hydration products in the composite system [24]. The depletion of Ca^{2+} in turn promoted the dissolution of the BOF slag. The enhancement of the early compressive strength of the BOF slag-cement mortar by the incorporation of iron tailings was not significant. Cement pastes with ternary SCMs comprising BOF slag, lithium slag, and iron tailings exhibited a higher presence of C-S-H gels, resulting in a more compact arrangement between the hydration products and the remaining unreacted particles. Iron tailings were used as fillers and acted as nucleation agents to accelerate the reaction of BOF slag and lithium slag in the cement paste. BOF slag, lithium slag, and iron tailings in the presence of DEIPA produced a synergistic effect, consuming more $\text{Ca}(\text{OH})_2$ and increasing the compressive strength. Future studies will focus on the effect of the DEIPA dosage on the properties of BOF slag-based cementitious materials.

4. Conclusions

This study investigated the effect mechanism of DEIPA and typical SCM on the hydration of BOF slag cement pastes. The fluidity, compressive strength, pore solution pH, and hydration products of BOF slag-based composite cementitious materials were discussed. The enhancement mechanism of BOF slag cement paste by organic alcohol amines and typical SCMs was revealed. The following conclusions were drawn:

1. The incorporation of DEIPA increased the early compressive strength of the BOF slag-cement mortar, but the later enhancement was small. DEIPA changed C-S-H from fibrous to flocculent in the BOF slag-cement mortar and accelerated the transition from AFt to AFm. DEIPA promoted the pozzolanic reaction of the composite system.
2. SCMs enhanced the hydration of BOF slag-cement paste when combined with DEIPA. The presence of SO_3 in lithium slag facilitated AFt formation, accelerated BOF slag reactions, and improved the BOF slag-cement system's compressive strength. The iron tailings showed little enhancement of the early strength of the BOF slag-cement mortar, which was attributed to the lower activity of BOF slag, serving primarily as a filler.
3. The cement mortar containing BOF slag, lithium slag, and iron tailings achieved a high compressive strength. The BOF slag, lithium slag, and iron tailings produced a synergistic effect in the cement mortar in the presence of DEIPA. The SCMs underwent a pozzolanic reaction, yielding additional hydration products.

Author Contributions: H.W.: Conceptualization, Investigation, Writing—original draft. X.G.: Conceptualization, Methodology, Investigation. X.X.: Conceptualization, Resources. J.L.: Resources. Z.Z.: Conceptualization. S.W.: Methodology, Supervision. All authors have read and agreed to the published version of the manuscript.

Funding: This research was funded by the National Key Research and Development Program of China (2023YFC3904303), National Natural Science Foundation of China (52234004), Science and Technology Plan Project of Shenyang (22322302), and the Shenyang major core key technology research and development special (20-202-4-39).

Data Availability Statement: The data presented in this study are available on request from the corresponding author. The data are not publicly available due to the nature of this research, participants of this study did not agree for their data to be shared publicly, so supporting data is not available.

Acknowledgments: The authors would like to thank Weiliang Huang from Shiyanjia Lab (www.shiyanjia.com) for the XRD analysis.

Conflicts of Interest: The authors declare that they have no known competing financial interests or personal relationships that could have appeared to influence the work reported in this paper.

References

1. Li, X.D.; Mehdizadeh, H.; Ling, T.C. Environmental, economic and engineering performances of aqueous carbonated steel slag powders as alternative material in cement pastes: Influence of particle size. *Sci. Total Environ.* **2023**, *903*, 11. [CrossRef] [PubMed]
2. Kaja, A.M.; Schollbach, K.; Melzer, S.; van der Laan, S.R.; Brouwers, H.J.H.; Yu, Q.L. Hydration of potassium citrate-activated BOF slag. *Cem. Concr. Res.* **2021**, *140*, 106291. [CrossRef]
3. Zepper, J.C.O.; van der Laan, S.R.; Schollbach, K.; Brouwers, H.J.H. Reactivity of BOF slag under autoclaving conditions. *Constr. Build. Mater.* **2023**, *364*, 14. [CrossRef]
4. Zhu, H.J.; Ma, M.Y.; He, X.Y.; Zheng, Z.Q.; Su, Y.; Yang, J.; Zhao, H. Effect of wet-grinding steel slag on the properties of Portland cement: An activated method and rheology analysis. *Constr. Build. Mater.* **2021**, *286*, 122823. [CrossRef]
5. Gencil, O.; Karadag, O.; Oren, O.H.; Bilir, T. Steel slag and its applications in cement and concrete technology: A review. *Constr. Build. Mater.* **2021**, *283*, 122783. [CrossRef]
6. Hou, J.; Liu, J. Hydration activity and mechanical properties of steel slag used as cementitious materials. *Environ. Prog. Sustain. Energy* **2021**, *41*, e13756. [CrossRef]
7. Nunes, V.A.; Borges, P.H.R. Recent advances in the reuse of steel slags and future perspectives as binder and aggregate for alkali-activated materials. *Constr. Build. Mater.* **2021**, *281*, 122605. [CrossRef]
8. Zhang, T.; Ma, B.; Wu, S.; Jin, Z.; Wang, J. Mechanical properties and hydration process of steel slag-cement binder containing nano-SiO₂. *Constr. Build. Mater.* **2022**, *314*, 125660. [CrossRef]
9. Brand, A.S.; Fanijo, E.O. A Review of the Influence of Steel Furnace Slag Type on the Properties of Cementitious Composites. *Appl. Sci.* **2020**, *10*, 8210. [CrossRef]
10. Rashad, A.M. A synopsis manual about recycling steel slag as a cementitious material. *J. Mater. Res. Technol.* **2019**, *8*, 4940–4955. [CrossRef]
11. Zhuang, S.Y.; Wang, Q. Inhibition mechanisms of steel slag on the early-age hydration of cement. *Cem. Concr. Res.* **2021**, *140*, 14. [CrossRef]
12. Wang, G.; Wang, Y.H.; Gao, Z.L. Use of steel slag as a granular material: Volume expansion prediction and usability criteria. *J. Hazard. Mater.* **2010**, *184*, 555–560. [CrossRef]
13. Jiang, J.; Lu, X.L.; Niu, T.; Hu, Y.Y.; Wu, J.M.; Cui, W.Y.; Zhao, D.G.; Ye, Z.M. Performance optimization and hydration characteristics of BOF slag-based autoclaved aerated concrete (AAC). *Cem. Concr. Comp.* **2022**, *134*, 11. [CrossRef]
14. Li, J.J.; Ni, W.; Wang, X.; Zhu, S.T.; Wei, X.L.; Jiang, F.X.; Zeng, H.; Hitch, M. Mechanical activation of medium basicity steel slag under dry condition for carbonation curing. *J. Build. Eng.* **2022**, *50*, 15. [CrossRef]
15. Wu, J.; Liu, Q.W.; Deng, Y.F.; Yu, X.B.; Feng, Q.; Yan, C. Expansive soil modified by waste steel slag and its application in subbase layer of highways. *Soils Found.* **2019**, *59*, 955–965. [CrossRef]
16. Xiao, B.L.; Wen, Z.J.; Miao, S.J.; Gao, Q. Utilization of steel slag for cemented tailings backfill: Hydration, strength, pore structure, and cost analysis. *Case Stud. Constr. Mater.* **2021**, *15*, 11. [CrossRef]
17. Sun, J.W.; Chen, Z.H. Effect of silicate modulus of water glass on the hydration of alkali-activated converter steel slag. *J. Therm. Anal. Calorim.* **2019**, *138*, 47–56. [CrossRef]
18. Wang, H.; Gu, X.; Liu, J.; Zhu, Z.; Wang, S.; Xu, X.; Nehdi, M.L. Synergistic effects of steel slag and lithium slag in carbonation-cured cement pastes: Carbonation degree, strength and microstructure. *J. Build. Eng.* **2024**, *85*, 108706. [CrossRef]
19. Sun, X.G.; Liu, J.; Zhao, Y.Q.; Zhao, J.H.; Li, Z.H.; Sun, Y.; Qiu, J.P.; Zheng, P.K. Mechanical activation of steel slag to prepare supplementary cementitious materials: A comparative research based on the particle size distribution, hydration, toxicity assessment and carbon dioxide emission. *J. Build. Eng.* **2022**, *60*, 19. [CrossRef]
20. Zhang, S.F.; Niu, D.T. Hydration and mechanical properties of cement-steel slag system incorporating different activators. *Constr. Build. Mater.* **2023**, *363*, 12. [CrossRef]
21. Xu, Z.Q.; Li, W.F.; Sun, J.F.; Hu, Y.Y.; Xu, K.; Ma, S.H.; Shen, X.D. Research on cement hydration and hardening with different alkanolamines. *Constr. Build. Mater.* **2017**, *141*, 296–306. [CrossRef]
22. Huo, B.B.; Li, B.L.; Huang, S.Y.; Chen, C.; Zhang, Y.M.; Banthia, N. Hydration and soundness properties of phosphoric acid modified steel slag powder. *Constr. Build. Mater.* **2020**, *254*, 9. [CrossRef]
23. Huo, B.B.; Li, B.L.; Chen, C.; Zhang, Y.M. Surface etching and early age hydration mechanisms of steel slag powder with formic acid. *Constr. Build. Mater.* **2021**, *280*, 11. [CrossRef]
24. Wang, J.F.; Chang, L.; Yue, D.Y.; Zhou, Y.F.; Liu, H.; Wang, Y.L.; Yang, S.G.; Cui, S.P. Effect of chelating solubilization via different alkanolamines on the dissolution properties of steel slag. *J. Clean. Prod.* **2022**, *365*, 11. [CrossRef]

25. Ma, B.G.; Zhang, T.; Tan, H.B.; Liu, X.H.; Mei, J.P.; Qi, H.H.; Jiang, W.B.; Zou, F.B. Effect of triisopropanolamine on compressive strength and hydration of cement-fly ash paste. *Constr. Build. Mater.* **2018**, *179*, 89–99. [[CrossRef](#)]
26. Li, C.B.; Ma, B.G.; Tan, H.B.; Zhang, T.; Liu, X.H.; Chen, P. Effect of triisopropanolamine on chloride binding of cement paste with ground-granulated blast furnace slag. *Constr. Build. Mater.* **2020**, *256*, 119494. [[CrossRef](#)]
27. Jiang, J.; Ye, Z.; Wu, J.; Yang, Q.; Li, Q.; Kong, X. Impact of triethanolamine on the hydration of Portland cement in the presence of high pozzolanic activity supplementary cementitious materials. *Cem. Concr. Compos.* **2024**, *147*, 105435. [[CrossRef](#)]
28. Ma, S.H.; Li, W.F.; Zhang, S.B.; Hu, Y.Y.; Shen, X.D. Study on the hydration and microstructure of Portland cement containing diethanol-isopropanolamine. *Cem. Concr. Res.* **2015**, *67*, 122–130. [[CrossRef](#)]
29. Liu, H.Q.; Zhang, Y.; Liu, J.L.; Feng, Z.X.; Kong, S. Comparative Study on Chloride Binding Capacity of Cement-Fly Ash System and Cement-Ground Granulated Blast Furnace Slag System with Diethanol-Isopropanolamine. *Materials* **2020**, *13*, 4103. [[CrossRef](#)]
30. Liu, J.; Wang, D. Influence of steel slag-silica fume composite mineral admixture on the properties of concrete. *Powder Technol.* **2017**, *320*, 230–238. [[CrossRef](#)]
31. Zhang, L.; Wang, Q.; Zheng, Y.; Cang, Z.; Gisele, K.; Yu, C.; Cang, D. Synergistic effect and mechanism of waste glass on the mechanical properties and autoclave stability of cementitious materials containing steel slag. *Constr. Build. Mater.* **2021**, *311*, 125295. [[CrossRef](#)]
32. Hao, X.S.; Liu, X.M.; Zhang, Z.Q.; Zhang, W.; Lu, Y.; Wang, Y.G.; Yang, T.Y. In-depth insight into the cementitious synergistic effect of steel slag and red mud on the properties of composite cementitious materials. *J. Build. Eng.* **2022**, *52*, 13. [[CrossRef](#)]
33. Lothenbach, B.; Scrivener, K.; Hooton, R.D. Supplementary cementitious materials. *Cem. Concr. Res.* **2011**, *41*, 1244–1256. [[CrossRef](#)]
34. Sun, J.; Zhang, P. Effects of different composite mineral admixtures on the early hydration and long-term properties of cement-based materials: A comparative study. *Constr. Build. Mater.* **2021**, *294*, 123547. [[CrossRef](#)]
35. Juilland, P.; Gallucci, E.; Flatt, R.; Scrivener, K. Dissolution theory applied to the induction period in alite hydration. *Cem. Concr. Res.* **2010**, *40*, 831–844. [[CrossRef](#)]
36. Liao, Y.S.; Wang, S.C.; Wang, K.J.; Al Qunaynah, S.; Wan, S.H.; Yuan, Z.X.; Xu, P.F.; Tang, S.W. A study on the hydration of calcium aluminate cement pastes containing silica fume using non-contact electrical resistivity measurement. *J. Mater. Res. Technol.-JMRT* **2023**, *24*, 8135–8149. [[CrossRef](#)]
37. Tang, S.W.; Cai, R.J.; He, Z.; Cai, X.H.; Shao, H.Y.; Li, Z.J.; Yang, H.M.; Chen, E. Continuous Microstructural Correlation of Slag/Superplasticizer Cement Pastes by Heat and Impedance Methods via Fractal Analysis. *Fractals-Complex Geom. Patterns Scaling Nat. Soc.* **2017**, *25*, 15. [[CrossRef](#)]
38. Yang, H.; Zhang, S.; Wang, L.; Chen, P.; Shao, D.; Tang, S.; Li, J. High-ferrite Portland cement with slag: Hydration, microstructure, and resistance to sulfate attack at elevated temperature. *Cem. Concr. Comp.* **2022**, *130*, 17. [[CrossRef](#)]
39. Gu, X.W.; Liu, B.N.; Li, Z.J.; Wang, H.; Liu, J.P.; Nehdi, M.L.; Zhang, Y.N. Mechanical grinding kinetics and particle packing novel characterization of iron ore tailings as inert filler for cement mortar. *J. Build. Eng.* **2023**, *78*, 17. [[CrossRef](#)]
40. Yang, M.; Sun, J.; Dun, C.; Duan, Y.; Meng, Z. Cementitious activity optimization studies of iron tailings powder as a concrete admixture. *Constr. Build. Mater.* **2020**, *265*, 120760. [[CrossRef](#)]
41. Yao, G.; Wang, Q.; Wang, Z.M.; Wang, J.X.; Lyu, X.J. Activation of hydration properties of iron ore tailings and their application as supplementary cementitious materials in cement. *Powder Technol.* **2020**, *360*, 863–871. [[CrossRef](#)]
42. Xu, X.C.; Wang, F.D.; Gu, X.W.; Zhao, Y.Q. Mechanism of Different Mechanically Activated Procedures on the Pozzolanic Reactivity of Binary Supplementary Cementitious Materials. *Minerals* **2022**, *12*, 1365. [[CrossRef](#)]
43. Gu, X.W.; Zhang, W.F.; Zhang, X.L.; Li, X.H.; Qiu, J.P. Hydration characteristics investigation of iron tailings blended ultra high performance concrete: The effects of mechanical activation and iron tailings content. *J. Build. Eng.* **2022**, *45*, 8. [[CrossRef](#)]
44. Cheng, Y.H.; Huang, F.; Li, W.C.; Liu, R.; Li, G.L.; Wei, J.M. Test research on the effects of mechanochemically activated iron tailings on the compressive strength of concrete. *Constr. Build. Mater.* **2016**, *118*, 164–170. [[CrossRef](#)]
45. Lv, X.D.; Shen, W.G.; Wang, L.; Dong, Y.; Zhang, J.F.; Xie, Z.Q. A comparative study on the practical utilization of iron tailings as a complete replacement of normal aggregates in dam concrete with different gradation. *J. Clean. Prod.* **2019**, *211*, 704–715. [[CrossRef](#)]
46. Han, F.H.; Luo, A.; Liu, J.H.; Zhang, Z.Q. Properties of high-volume iron tailing powder concrete under different curing conditions. *Constr. Build. Mater.* **2020**, *241*, 118108. [[CrossRef](#)]
47. Huang, S.Z.; Wang, Y.; Zhang, L.; Zhu, S.J.; Ma, Z.F.; Cui, Q.; Wang, H.Y. Insight into the kinetic behavior of microwave-assisted synthesis of NaX zeolite from lithium slag. *New J. Chem.* **2023**, *47*, 14335–14343. [[CrossRef](#)]
48. Zhang, T.; Ma, B.; Tan, H.; Liu, X.; Chen, P.; Luo, Z. Effect of TIPA on mechanical properties and hydration properties of cement-lithium slag system. *J. Environ. Manag.* **2020**, *276*, 111274. [[CrossRef](#)] [[PubMed](#)]
49. Tan, H.; Li, M.; He, X.; Su, Y.; Yang, J.; Zhao, H. Effect of wet grinded lithium slag on compressive strength and hydration of sulphoaluminate cement system. *Constr. Build. Mater.* **2021**, *267*, 120465. [[CrossRef](#)]
50. Tan, H.; Zhang, X.; He, X.; Guo, Y.; Deng, X.; Su, Y.; Yang, J.; Wang, Y. Utilization of lithium slag by wet-grinding process to improve the early strength of sulphoaluminate cement paste. *J. Clean. Prod.* **2018**, *205*, 536–551. [[CrossRef](#)]
51. Gu, X.W.; Wang, H.Y.; Zhu, Z.G.; Liu, J.P.; Xu, X.C.; Wang, Q. Synergistic effect and mechanism of lithium slag on mechanical properties and microstructure of steel slag-cement system. *Constr. Build. Mater.* **2023**, *396*, 131768. [[CrossRef](#)]

52. Wang, H.; Gu, X.; Liu, J.; Zhu, Z.; Wang, S.; Xu, X.; Meng, J. Enhancement mechanism of micro-iron ore tailings on mechanical properties and hydration characteristics of cement-steel slag system. *J. Build. Eng.* **2023**, *79*, 107882. [[CrossRef](#)]
53. Chang, L.; Liu, H.; Wang, J.; Liu, H.; Song, L.; Wang, Y.; Cui, S. Effect of chelation via ethanol-diisopropanolamine on hydration of pure steel slag. *Constr. Build. Mater.* **2022**, *357*, 129372. [[CrossRef](#)]
54. Li, W.F.; Ma, S.H.; Zhang, S.B.; Shen, X.D. Physical and chemical studies on cement containing sugarcane molasses. *J. Therm. Anal Calorim.* **2014**, *118*, 83–91. [[CrossRef](#)]
55. GB/T 17671-2021; Test Method of Cement Mortar Strength (ISO Method). Standardization Administration of the People's Republic of China: Beijing, China, 2021.
56. Gu, X.; Ge, X.; Liu, J.; Song, G.; Wang, S.; Hu, Z.; Wang, H. Study on the synergistic effect of calcium carbide residue-fly ash enhanced desulphurisation gypsum under high temperature maintenance condition. *Constr. Build. Mater.* **2024**, *412*, 134706. [[CrossRef](#)]
57. Yang, S.; Wang, J.; Cui, S.; Liu, H.; Wang, X. Impact of four kinds of alkanolamines on hydration of steel slag-blended cementitious materials. *Constr. Build. Mater.* **2017**, *131*, 655–666. [[CrossRef](#)]
58. Liao, Y.S.; Yao, J.X.; Deng, F.; Li, H.; Wang, K.J.; Tang, S.W. Hydration behavior and strength development of supersulfated cement prepared by calcined phosphogypsum and slaked lime. *J. Build. Eng.* **2023**, *80*, 16. [[CrossRef](#)]
59. Wang, S.Y.; Gu, X.W.; Liu, J.P.; Zhu, Z.G.; Wang, H.Y.; Ge, X.W.; Xu, X.C.; Nehdi, M.L. Modulation of the workability and Ca/Si/Al ratio of cement-metakaolin cementitious material system by using fly ash: Synergistic effect and hydration products. *Constr. Build. Mater.* **2023**, *404*, 15. [[CrossRef](#)]
60. Kang, H.; Yang, J.; Kim, S.; Lim, A.; Moon, J. Mechanochemical activation for transforming bottom ash to reactive supplementary cementitious material. *Constr. Build. Mater.* **2024**, *411*, 134523. [[CrossRef](#)]
61. Gu, X.; Wang, H.; Liu, J.; Zhu, Z.; Wang, S.; Xu, X. Synergistic effects of steel slag and metakaolin in cementitious systems: Packing properties, strength, and microstructure. *Constr. Build. Mater.* **2024**, *411*, 134395. [[CrossRef](#)]
62. Kapeluszna, E.; Kotwica, L.; Rózycka, A.; Golek, L. Incorporation of Al in C-A-S-H gels with various Ca/Si and Al/Si ratio: Microstructural and structural characteristics with DTA/TG, XRD, FTIR and TEM analysis. *Constr. Build. Mater.* **2017**, *155*, 643–653. [[CrossRef](#)]
63. Geng, Z.; Tang, S.; Wang, Y.; Hubao, A.; He, Z.; Wu, K.; Wang, L. Stress relaxation properties of calcium silicate hydrate: A molecular dynamics study. *J. Zhejiang Univ.-Sci. A* **2024**, *25*, 97–115. [[CrossRef](#)]
64. Tang, S.; Wang, Y.; Geng, Z.; Xu, X.; Yu, W.; Hubao, A.; Chen, J. Structure, Fractality, Mechanics and Durability of Calcium Silicate Hydrates. *Fractal Fract.* **2021**, *5*, 47. [[CrossRef](#)]
65. Li, Y.; Zhang, H.; Huang, M.H.; Yin, H.B.; Jiang, K.; Xiao, K.T.; Tang, S.W. Influence of Different Alkali Sulfates on the Shrinkage, Hydration, Pore Structure, Fractal Dimension and Microstructure of Low-Heat Portland Cement, Medium-Heat Portland Cement and Ordinary Portland Cement. *Fractal Fract.* **2021**, *5*, 79. [[CrossRef](#)]
66. Zhou, Y.F.; Li, W.W.; Peng, Y.X.; Tang, S.W.; Wang, L.; Shi, Y.; Li, Y.; Wang, Y.; Geng, Z.C.; Wu, K. Hydration and Fractal Analysis on Low-Heat Portland Cement Pastes Using Thermodynamics-Based Methods. *Fractal Fract.* **2023**, *7*, 606. [[CrossRef](#)]

Disclaimer/Publisher's Note: The statements, opinions and data contained in all publications are solely those of the individual author(s) and contributor(s) and not of MDPI and/or the editor(s). MDPI and/or the editor(s) disclaim responsibility for any injury to people or property resulting from any ideas, methods, instructions or products referred to in the content.